pubs.acs.org/acschemicalbiology

Articles

Metabolically Activated Proteostasis Regulators Protect against Glutamate Toxicity by Activating NRF2

Jessica D. Rosarda, Kelsey R. Baron, Kayla Nutsch, Gabriel M. Kline, Caroline Stanton, Jeffery W. Kelly, Michael J. Bollong, and R. Luke Wiseman*

Cite This: *ACS Chem. Biol.* 2021, 16, 2852–2863

Read Online

ACCESS | Metrics & More | Article Recommendations | Supporting Information

ABSTRACT: The extracellular accumulation of glutamate is a pathologic hallmark of numerous neurodegenerative diseases including ischemic stroke and Alzheimer's disease. At high extracellular concentrations, glutamate causes neuronal damage by promoting oxidative stress, which can lead to cellular death. This has led to significant interest in developing pharmacologic approaches to mitigate the oxidative toxicity caused by high levels of glutamate. Here, we show that the small molecule proteostasis regulator AA147 protects against glutamate-induced cell death in a neuronal-derived cell culture model. While originally developed as an activator of the activating transcription factor 6 (ATF6) arm of the unfolded protein response, this AA147-dependent protection against glutamate toxicity is primarily mediated through activation of the NRF2-regulated oxidative stress response. We demonstrate that AA147 activates NRF2 selectively in neuronal-derived cells through a mechanism involving metabolic activation to a reactive electrophile and covalent modification of KEAP1—a mechanism analogous to that involved in the AA147-dependent activation of ATF6. These results define the potential for AA147 to protect against glutamate-induced oxidative toxicity and highlight the potential for metabolically activated proteostasis regulators like AA147 to activate both protective ATF6 and NRF2 stress-responsive signaling pathways to mitigate oxidative damage associated with diverse neurologic diseases.

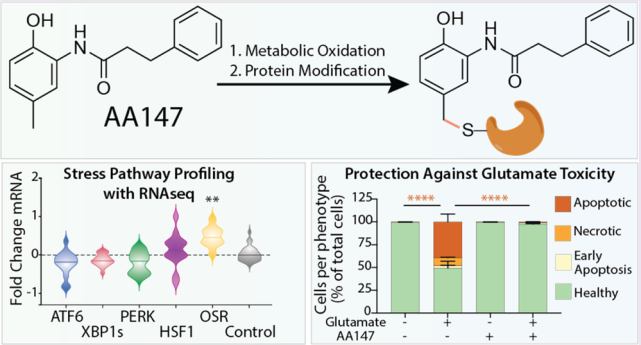

INTRODUCTION

Glutamate is an essential excitatory neurotransmitter involved in nervous system function. The controlled release of glutamate into the synapse is critical for neuronal signaling.[1,2] However, acute or chronic events that cause pathologic depolarization of neuronal cell membranes lead to an uncontrolled release of glutamate into the extracellular space, causing aberrant excitotoxic and oxidative signaling that can lead to cell death.[1−3] High levels of extracellular glutamate trigger a cascade of excitatory signaling through the excessive stimulation of neuronal *N*-methyl-D-aspartate (NMDA) receptors, which release additional glutamate into the synapse.[2,4] Neurons decrease extracellular glutamate levels by reversing the function of the XC- antiporter, which then imports glutamate and exports cystine.[5,6] Cystine is a vital precursor to the intracellular antioxidant glutathione, and prolonged reversal of the XC- system depletes glutathione stores.[7] Therefore, high levels of extracellular glutamate result in decreased antioxidant capacity within the cell, causing oxidative stress that can lead to cell death independent of NMDA receptor activation.[6,8] Limiting excitotoxicity using NMDA receptor antagonists protects against neurodegeneration in multiple neurologic disorders, including human and mouse models of Alzheimer's disease and ischemic stroke.[3,9,10] However, inhibition of these receptors can be problematic, as it also disrupts physiologic excitatory signaling.[3,11] An alternative approach to treat these disorders is to limit the cell death caused by glutamate-induced oxidative damage.[12,13]

We recently identified the compound AA147, which is protective against reactive oxygen species (ROS)-mediated damage caused by ischemia and reperfusion (I/R) injury in both cells and mice.[14,15] Administration of AA147 improved outcomes in mouse models of cardiac and kidney I/R injury. Further, AA147 administered either prior to the onset of ischemia or at the time of reperfusion reduced both the infarct size and neurological dysfunction in mice subjected to cerebral I/R.[14] Glutamate toxicity is a major contributor to neurologic damage following an ischemic stroke, which suggested that

Received: October 13, 2021
Accepted: October 29, 2021
Published: November 19, 2021

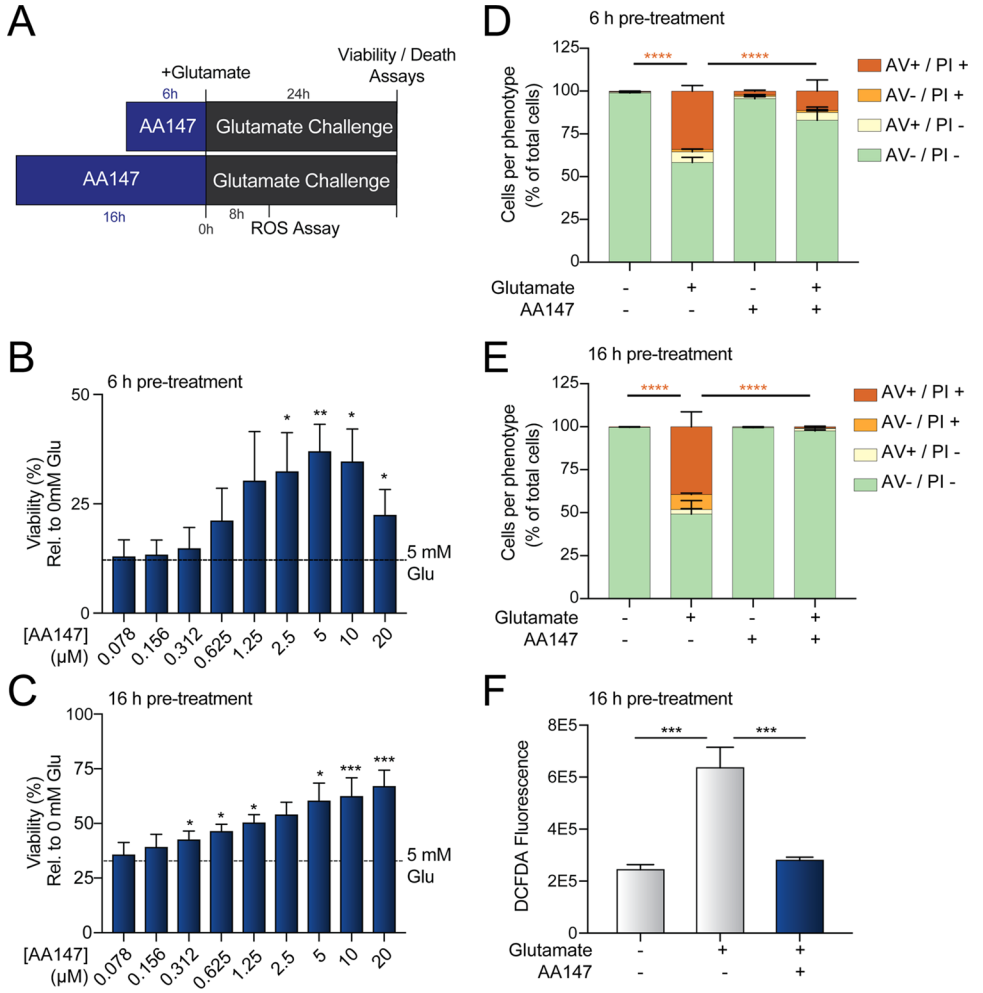

Figure 1. AA147 protects against glutamate-induced oxidative toxicity in HT22 cells. (A) Schematic of the AA147 pretreatment conditions and glutamate challenge. (B, C) Viability, measured by MTT assay, of HT22 cells pretreated with the indicated dose of AA147 for 6 h (B) or 16 h (C) and then challenged with glutamate (5 mM) for 24 h. Viability is shown as a percent relative to vehicle-treated cells where glutamate was not added. Error bars show standard error of the mean (SEM) for $n = 4$ (B) or $n = 5$ (C) replicates. *$p < 0.05$, **$p < 0.01$, ***$p < 0.001$ for two-tailed paired Student's t test comparing samples treated with AA147 with an equivalent volume of vehicle. (D, E). Quantification of HT22 cells pretreated with AA147 for 6 h (D) or 16 h (E) and then challenged with glutamate (5 mM) for 24 h and then stained with Annexin V (AV) and/or propidium iodide (PI) shown as a percentage of total cells counted per experiment. Error bars show SEM for $n = 3$ replicates. ****$p < 0.0001$ for ordinary one-way analysis of variance (ANOVA) with Tukey correction for multiple comparisons between conditions. (F) Geometric mean of CM-H2DCFDA fluorescence of HT22 cells pretreated with AA147 (10 μM) for 16 h and then challenged with glutamate (5 mM) for 8 h, as indicated. Error bars show SEM for $n = 3$ replicates. ***$p < 0.001$ for ordinary one-way ANOVA with Tukey correction for multiple comparisons between conditions.

AA147 could decrease cerebral I/R damage by ameliorating glutamate toxicity.[3,11]

AA147 was originally developed as a pharmacologic activator of the activating transcription factor 6 (ATF6) signaling pathway within the unfolded protein response (UPR).[15,16] Activation of ATF6 upregulates a transcriptional response during conditions of endoplasmic reticulum (ER) stress through a process involving increased trafficking of full-length ATF6 to the Golgi and subsequent proteolytic release of the active N-terminal ATF6 transcription factor domain by site 1 (S1P) and site 2 (S2P) proteases.[16,17] Upon nuclear localization, ATF6 induces the expression of multiple ER proteostasis factors including protein chaperones, such as BiP, GRP94, and PDIA4, as well as redox factors, such as HMOX1.[15,16,18,19] AA147 induces the nuclear translocation of ATF6 through a mechanism involving compound metabolic activation to a reactive electrophile and subsequent covalent modification of a subset of ER-localized protein disulfide isomerases (PDIs) involved in regulating the trafficking of ATF6 to the Golgi.[20] This mechanism allows AA147 to preferentially activate the ATF6 arm of the UPR in both cell culture models and in vivo.[15,16]

ATF6 transcriptional activity is protective in models of etiologically diverse diseases, making this pathway an attractive therapeutic target for disease intervention.[14,16,21−24] Consistent with this, pharmacologic activation of ATF6 with AA147 is protective in models of numerous diseases. For example, AA147-dependent ATF6 activation is protective in mouse models of myocardial infarction and cardiac arrest, as well as iPSC-derived models of the eye disease achromatopsia.[14,24−26] However, AA147 can also promote protection through ATF6-independent mechanisms. AA147-dependent covalent modification of PDIs, an upstream step involved in AA147-dependent ATF6 activation,[20] is sufficient to reduce the

https://doi.org/10.1021/acschembio.1c00810
ACS Chem. Biol. 2021, 16, 2852−2863

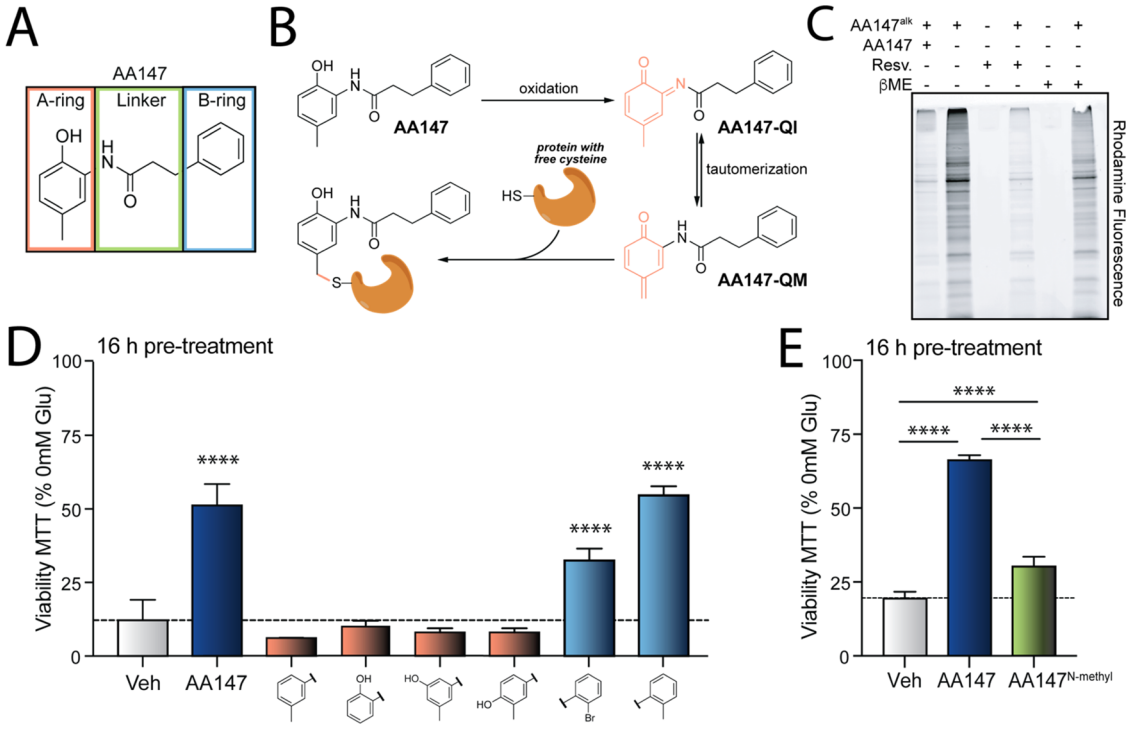

Figure 2. 2-Amino-*p*-cresol substructure of AA147 is required to protect HT22 cells against glutamate-induced oxidative toxicity. (A) Structure of AA147 with its three components—the A-ring, linker, and B-ring, highlighted. The A-ring (orange) contains the 2-amino-*p*-cresol moiety. (B) Schematic showing the mechanism of AA147 metabolic activation to a quinone-imine (AA147-QI) or quinone methide (AA147-QM) and subsequent covalent protein modification. Adapted with permission from (20) ©2018 Paxman et al., licensed under CC BY 4.0. (C) Rhodamine gel image of HT22 cells treated with $AA147^{alk}$ (10 μM) for 16 h, in competition with AA147 (50 μM) and in the presence or absence of the P450 inhibitor resveratrol (10 μM) or β-mercaptoethanol (βME; 55 μM). (D) Viability, measured by MTT, of HT22 cells pretreated with the indicated AA147 analogue (10 μM) for 16 h and challenged with glutamate (5 mM) for 24 h. Viability is shown as a percent of HT22 cells pretreated with the respective analogue in the absence of glutamate. Error bars show standard deviation (SD) for $n = 3$ replicates. ****$p < 0.0001$ for ordinary one-way ANOVA comparing analogue-treated cells to vehicle-treated cells with Dunnett correction for multiple comparisons. (E) Viability, measured by MTT, of HT22 cells pretreated with AA147 (10 μM) or $AA147^{N\text{-methyl}}$ (10 μM) for 16 h and challenged with glutamate (5 mM) for 24 h. Viability is shown as a percent of HT22 cells pretreated with respective treatments in the absence of glutamate. Error bars show SD for $n = 5$ replicates. ****$p < 0.0001$ for ordinary one-way ANOVA comparing analogue with Tukey correction for multiple comparisons between conditions.

secretion and toxic aggregation of amyloidogenic immunoglobulin light chains associated with light chain amyloidosis independent of ATF6 signaling.[27] Further, AA147 protects the liver against viral infection through an ATF6-independent mechanism.[28] These results highlight that apart from ATF6 activation, AA147 can also protect against diverse pathologic insults through mechanisms independent of ATF6 activity.

Here, we sought to define the potential for AA147 to protect against glutamate-induced oxidative toxicity in HT22 cells, an immortalized cell line derived from hippocampal neurons lacking the NMDA receptors required for glutamate-induced excitotoxicity.[8] As the treatment of HT22 cells with glutamate thus induces oxidative stress independently of excitatory signaling, this cell line has been a widely used model to develop pharmacologic approaches to mitigate the oxidative toxicity caused by glutamate.[5,8,29] Here, we show that AA147 protects HT22 cells against glutamate-induced oxidative toxicity. Intriguingly, this protection is only partially dependent on ATF6 activation. Instead, AA147-dependent protection against glutamate-induced oxidative toxicity is primarily mediated through compound-dependent activation of the NRF2 oxidative stress response (OSR). Interestingly, structure−activity relationships indicate that AA147 activates NRF2 selectively in neuronal-derived cell lines through a mechanism involving compound metabolic activation and covalent targeting of the NRF2 regulatory protein KEAP1, a mechanism analogous to that involved in AA147-dependent ATF6 activation.[20] These results demonstrate that AA147 offers a unique opportunity to activate both adaptive ATF6 and NRF2 transcriptional signaling in neuronal cell models, revealing further insights into the molecular basis for protection afforded by this compound in different cell types. Further, our results demonstrate the broad potential for AA147 and related compounds to mitigate oxidative damage induced by pathologic insults through the coordinated regulation of two protective stress-responsive signaling pathways.

RESULTS AND DISCUSSION

AA147 Protects against Glutamate-Induced Oxidative Toxicity. We sought to define the potential of AA147 to reduce glutamate-induced oxidative toxicity in HT22 cells. We initially confirmed that AA147 activated the ATF6-selective ERSE-luciferase reporter (ERSE-LUC)[15] in HT22 cells with an EC_{50} of 3.6 μM (Figure S1A). Further, we showed that AA147 did not significantly influence HT22 cell viability (Figure S1B). These results are consistent with the AA147 activity observed in other cell models[15] and demonstrate that AA147 is active in HT22 cells. Next, we assessed whether AA147 reduces glutamate-induced oxidative toxicity in HT22 cells. Initially, we used the 3-(4,5-dimethylthiazol-2-yl)-2,5-diphenyltetrazo-

https://doi.org/10.1021/acschembio.1c00810
ACS Chem. Biol. 2021, 16, 2852−2863

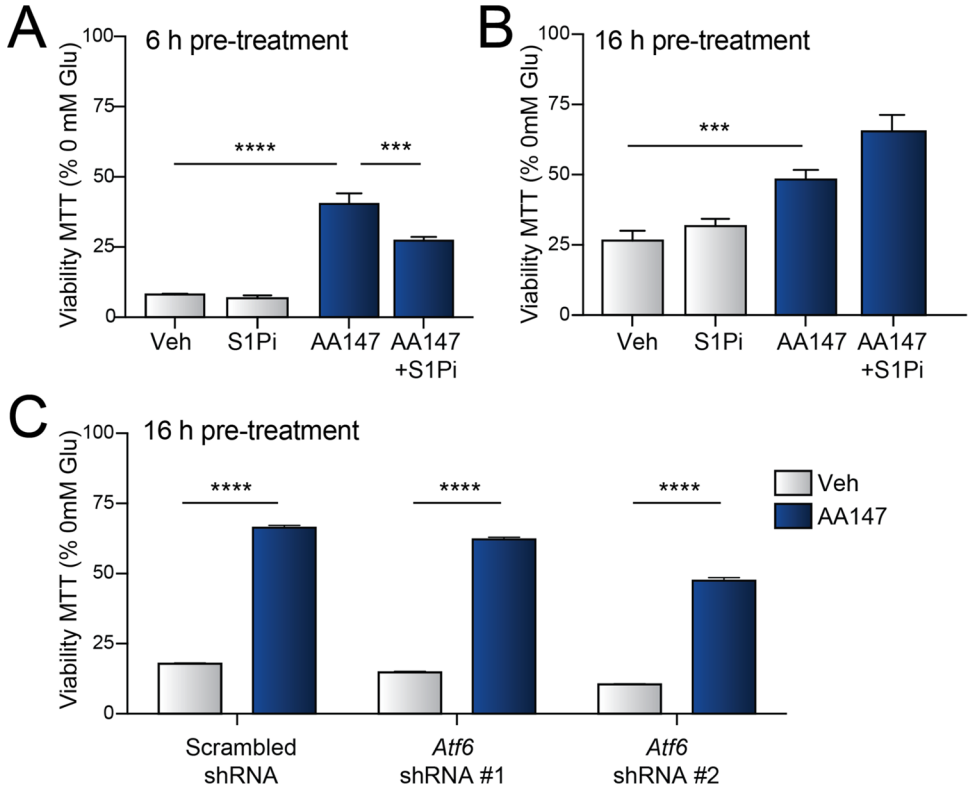

Figure 3. AA147-dependent activation of ATF6 modestly contributes to the AA147-dependent protection of HT22 cells against glutamate-induced oxidative toxicity. (A, B) Viability, measured by MTT, of HT22 cells pretreated with AA147 (10 μM) for 6 h (A) or 16 h (B) in the presence or absence of S1Pi (10 μM) and then challenged with glutamate (5 mM) for 24 h. Viability is shown as a percent relative to cells treated with the respective treatment in the absence of glutamate. Error bars show SD for $n = 3$. ***$p < 0.001$, ****$p < 0.0001$ for two-way ANOVA with Tukey correction for multiple testing between conditions. (C) Viability, measured by MTT assay, of HT22 cells expressing scrambled or *Atf6* shRNA pretreated for 16 h with AA147 (10 μM) and then challenged with glutamate (5 mM) for 24 h. Viability is shown as a percent relative to cells with the respective treatment in the absence of glutamate. Error bars show SD for $n = 3$. ****$p < 0.0001$ for two-way ANOVA with Tukey correction for multiple testing between conditions.

lium bromide (MTT) assay to monitor the viability of HT22 cells pretreated with AA147 for different times and then challenged with glutamate for 24 h (Figure 1A). We found that 24 h treatment with glutamate reduced the viability of HT22 cells between 65 and 90%, as measured by MTT (Figure S1C). Addition of AA147 concurrently with the glutamate challenge did not improve the viability of glutamate-treated cells (Figure S1C). However, pretreatment with AA147 for 6 or 16 h prior to the glutamate challenge showed dose-dependent increases in the viability of glutamate-treated HT22 cells (Figure 1B,C). AA147 similarly demonstrated protection when monitoring glutamate-induced cell death in HT22 cells by Annexin V (AV) and propidium iodide (PI) staining, where pretreatment with AA147 for 6 or 16 h reduced the population of Annexin V/PI positive cells (Figures 1D,E and S1D,E). In this assay, 16 h pretreatment proved to be most effective at mitigating cell death.

AA147 reduces toxicity induced by oxidative stress in several cell types by decreasing the reactive oxygen species (ROS)-associated damage.[14] Thus, we sought to determine if AA147 reduced ROS levels in glutamate-treated HT22 cells. HT22 cells show a significant increase in ROS 8 h after the addition of glutamate, as measured by DCFDA fluorescence (Figure 1F), consistent with published results.[29] Pretreatment with AA147 for 16 h significantly reduced DCFDA fluorescence in glutamate-challenged cells, indicating that AA147 reduces ROS accumulation in these cells. Collectively, these results demonstrate that AA147 attenuates glutamate-induced oxidative toxicity in HT22 cells.

The 2-Amino-*p*-cresol Substructure of AA147 Is Required for Protection against Glutamate Toxicity. AA147 consists of a 2-amino-*p*-cresol moiety (designated as the A-ring) linked to an aromatic B-ring via a hydrocarbon linker (Figure 2A).[15,20] Previous studies demonstrated that the 2-amino-*p*-cresol moiety is metabolically activated by ER-localized oxidases to form reactive electrophiles such as a quinone methide (AA147-QM) or quinone-imine (AA147-QI) (Figure 2B).[20] These electrophilic forms of AA147 covalently modify reactive cysteines on proteins predominantly localized to the endoplasmic reticulum (ER).[20] Initially, we asked whether AA147 covalently modified proteins in HT22 cells using an analogue of AA147 with an alkyne handle on the B-ring ($AA147^{alk}$) (Figure S2A) that allows monitoring of covalently modified proteins by "click chemistry".[20] $AA147^{alk}$ protected against glutamate-induced toxicity in HT22 cells (Figure S2B). We showed that $AA147^{alk}$ covalently modified proteins in HT22 cells by conjugating a rhodamine-azide to $AA147^{alk}$-modified proteins using a copper-catalyzed alkyne–azide cycloaddition reaction (Figure S2C). Cotreatment with a 5-fold excess of AA147 reduced $AA147^{alk}$ labeling, indicating that AA147 competes with $AA147^{alk}$ for binding to proteins in HT22 cells. Coadministration with resveratrol, a P450 inhibitor, or β-mercaptoethanol (βME), a free thiol-containing compound—two compounds previously shown to disrupt

https://doi.org/10.1021/acschembio.1c00810
ACS Chem. Biol. 2021, 16, 2852−2863

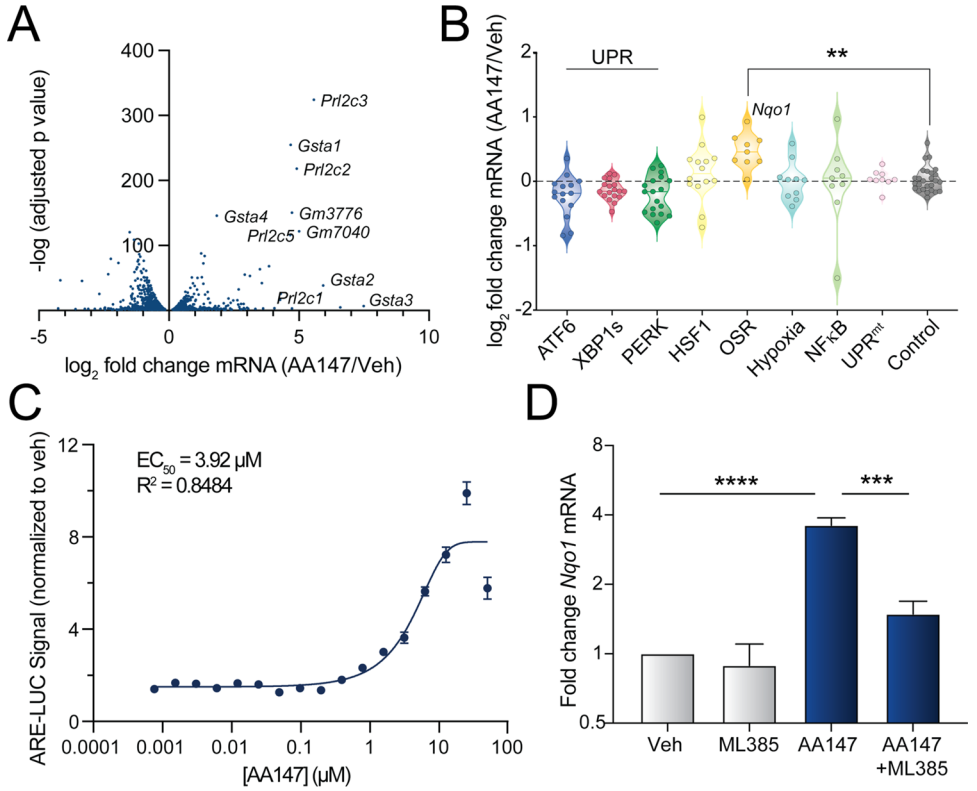

Figure 4. AA147 induces NRF2-dependent upregulation of oxidative stress response genes in HT22 cells. (A) Plot showing −log adj p-value vs $\log_2$ fold change (AA147/Veh) for genes identified in RNA-seq analysis of HT22 cells treated with vehicle or AA147 (10 μM) for 16 h. Select glutathione transferase and prolactin genes are indicated. Complete RNA-seq data is shown in Table S1. (B) Graph showing the expression of sets of genes regulated downstream of the ATF6, XBP1s, or PERK arms of the UPR, the HSF1-regulated heat shock response, the oxidative stress response (OSR), the hypoxia stress response, NFκB inflammatory signaling, and the mitochondrial unfolded protein response (UPR^{mt}), as well as a set of control genes. Gene sets are defined as previously described (34) and are shown in Table S2. $^{**}p < 0.01$ for one-way ANOVA comparing the expression of individual stress-induced transcription factor gene sets to the control gene set. (C) Luminescence in HT22 cells transiently expressing the antioxidant response element (ARE)-LUC reporter and treated with AA147 (10 μM) for 16 h. Luminescence is shown as a fold change relative to vehicle. Error bars show SEM for $n = 20$ replicates across two independent experiments; 95% CI = 3.239−4.182 μM, (D) Expression of the NRF2 target gene *Nqo1*, measured by qPCR, in HT22 cells treated with vehicle or AA147 (10 μM) in the presence or absence of ML385 (5 μM) for 16 h. Error bars show SEM for $n = 3$. $^{***}p < 0.001$, $^{****}p < 0.0001$ for two-way ANOVA with Tukey correction for multiple testing between conditions.

AA147-dependent oxidation and covalent modification of proteins[20]—reduces $AA147^{alk}$ protein labeling in HT22 cells (Figures 2C and S2D). Similarly, cotreatment with resveratrol or β-mercaptoethanol reduced AA147-dependent activation of the ERSE-LUC reporter in HT22 cells (Figure S2E). These results are identical to those observed in other cell types[20,27] and demonstrate that AA147 covalently modifies proteins in HT22 cells through a mechanism involving metabolic activation and covalent cysteine modification (Figure 2B).

Next, we further probed the dependence of AA147-dependent protection against glutamate-induced oxidative toxicity on the mechanism shown in Figure 2B using a series of AA147 analogues. As observed for ATF6 activation,[20] the treatment of HT22 cells for 16 h with compounds containing disruptions in the 2-amino-*p*-cresol A-ring structure required for metabolic activation did not protect against glutamate-induced toxicity (Figure 2D). However, modification of the B-ring at the ortho position with either a bromine or methyl group did not significantly impact AA147-dependent protection. Similar results were observed for cells treated for 6 h with AA147 analogues (Figure S2F). This structure−activity relationship is the same as that previously shown to regulate ATF6 activation in HEK293 cells.[20]

To further probe the potential contributions of the reactive, electrophilic forms of AA147 in the observed protection against glutamate toxicity (Figure 2B), we synthesized an AA147 analogue containing a tertiary amine on the linker amide ($AA147^{N\text{-methyl}}$; Figure S2G−K). This analogue disfavors oxidation to the reactive AA147-QI, although it could potentially be converted directly to AA147-QM through an alternative oxidation reaction. We found that $AA147^{N\text{-methyl}}$ showed significantly less protection against glutamate-induced toxicity, as compared to AA147, although a minimal amount of protection was still observed (Figure 2E). Combined, these results are consistent with a model whereby metabolic conversion of the A-ring domain of AA147 to a reactive AA147-QI is a critical step for the AA147-dependent protection against glutamate-induced toxicity in HT22 cells (Figure 2B).

AA147-Dependent ATF6 Activation Only Modestly Contributes to Protection against Glutamate-Induced Toxicity Observed in HT22 Cells. AA147 protects cardiomyocytes from oxidative insults through the activation of ATF6.[14] Thus, we sought to define the dependence of AA147-dependent protection against glutamate-induced oxidative toxicity on ATF6 activation. Initially, we used an

https://doi.org/10.1021/acschembio.1c00810
ACS Chem. Biol. 2021, 16, 2852−2863

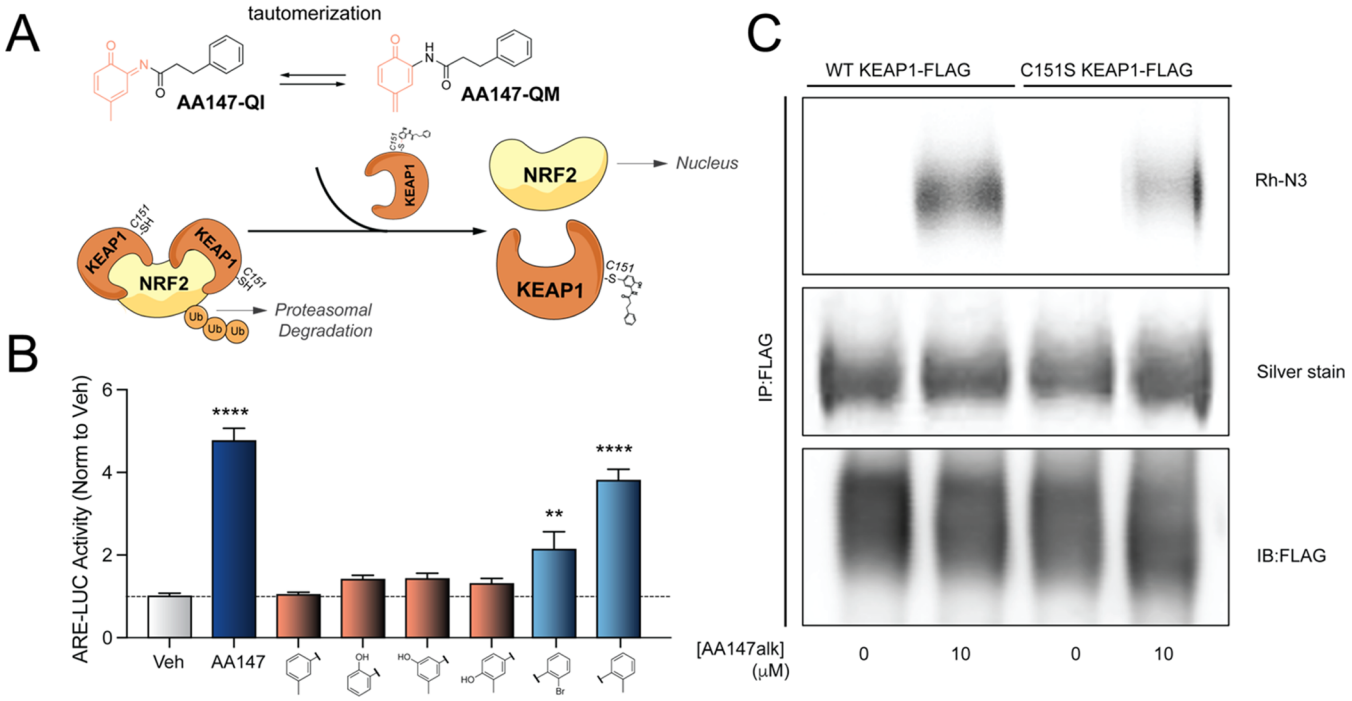

Figure 5. AA147 covalently modifies KEAP1, a regulator of NRF2 transcriptional activity. (A) Proposed model whereby the metabolically activated AA147 covalently modifies Cys151 on KEAP1 to reduce ubiquitination and allow nuclear localization of NRF2 to promote transcriptional activity. (B) Luminescence in HT22 cells transiently expressing the ARE-LUC NRF2 reporter treated with the indicated AA147 analogue (10 μM) for 16 h. Error bars show SEM for n = 20 replicates across two independent experiments. $^{**}p < 0.01$ and $^{****}p < 0.0001$ for ordinary one-way ANOVA against vehicle control with Dunnett correction for multiple comparisons. (C) Fluorescence image (top) and immunoblot (bottom) of FLAG immunopurifications prepared from HEK293T cells transiently overexpressing wild-type (WT) KEAP^{FT} or C151S KEAP^{FT} and treated for 16 h with AA147^{alk} (10μM). AA147^{alk}-modified proteins were conjugated to rhodamine-azide (Rh-N_3) by click chemistry (top), total protein was measured using silver stain (middle), and KEAP1:FLAG levels were confirmed using immunoblotting with FLAG antibody (bottom).

inhibitor of ATF6 activation, the S1P inhibitor PF429242 (S1Pi),[30] to define the importance of AA147-dependent ATF6 activation on the protection observed in glutamate-treated HT22 cells. We confirmed that S1Pi inhibited AA147-dependent induction of the ATF6 target *BiP*/*Hspa5* in HT22 cells by quantitative polymerase chain reaction (qPCR) and immunoblotting (Figure S3A,B). Next, we monitored the viability of HT22 cells pretreated with AA147 and S1Pi for 6 h or 16 h and then challenged with glutamate. Cotreatment with S1Pi modestly attenuated the AA147-dependent protection observed following a 6 h pretreatment (Figure 3A). Similarly, shRNA depletion of *Atf6* (Figure S3C) also modestly reduced protection observed following a 6 h treatment with AA147 (Figure S3D). These results suggested that AA147-dependent ATF6 activation contributes to protection from glutamate-induced oxidative toxicity observed at this time point. Despite this reduction in protection, ATF6 activation cannot explain the entirety of the observed effect following a 6 h pretreatment. In contrast, neither cotreatment with S1Pi (Figure 3B) nor *Atf6* depletion (Figures 3C and S3E) impacted AA147-dependent improvements in HT22 viability observed following a 16 h pretreatment. Combined, these results suggest that AA147-dependent ATF6 activation offers a limited contribution to the observed protection from glutamate-induced oxidative stress in HT22 cells.

AA147 Activates the Oxidative Stress Response in HT22 Cells. To better define the mechanistic basis of AA147-dependent protection against glutamate-induced oxidative toxicity, we performed RNA sequencing (RNA-seq) on HT22 cells treated with vehicle or AA147 for 16 h (Table S1). Despite observing a robust induction of the ATF6 target gene *BiP* following 6 h treatment (Figure S3A), RNA-seq showed that *BiP* expression was not increased following 16 h treatment with AA147 in these cells (Table S1). We confirmed this result by qPCR (Figure S4A). This is consistent with the transient AA147-dependent activation of ATF6 signaling observed in other cells.[15] However, we observed significant increases in the expression of genes associated with antioxidant activity in neuronal models, including prolactins (e.g., *Prl2c2*, *Prl2c3*) and glutathione transferases (e.g., *Gsta1*, *Gsta4*) in AA147-treated HT22 cells (Figure 4A).[31−33] Gene ontology (GO) analysis showed increases in antioxidant pathways, including glutathione transferase activity and prolactin receptor binding (Figure S4B). Further, when monitoring the expression of established gene sets associated with different stress-responsive signaling pathways,[34] only target genes involved in the oxidative stress response showed a coordinated upregulation of expression, as compared to control genes, in AA147-treated HT22 cells (Figure 4B and Table S2). Notably, transcriptional targets of ATF6 or other arms of the UPR (i.e., IRE1/XBP1s and PERK) were not induced in HT22 cells treated for 16 h with AA147 (Figure 4B and Table S2), again reflecting the transient nature of AA147-dependent activation of ATF6 in these cells.[15] These results suggest that AA147 induces an oxidative stress response in HT22 cells.

The oxidative stress response is primarily regulated by the transcription factor NRF2, which binds to antioxidant response element (ARE) sequences within the promoter region of target genes to induce their expression.[35,36] NRF2 activity protects against multiple different types of oxidative insults, including

https://doi.org/10.1021/acschembio.1c00810
ACS Chem. Biol. 2021, 16, 2852−2863

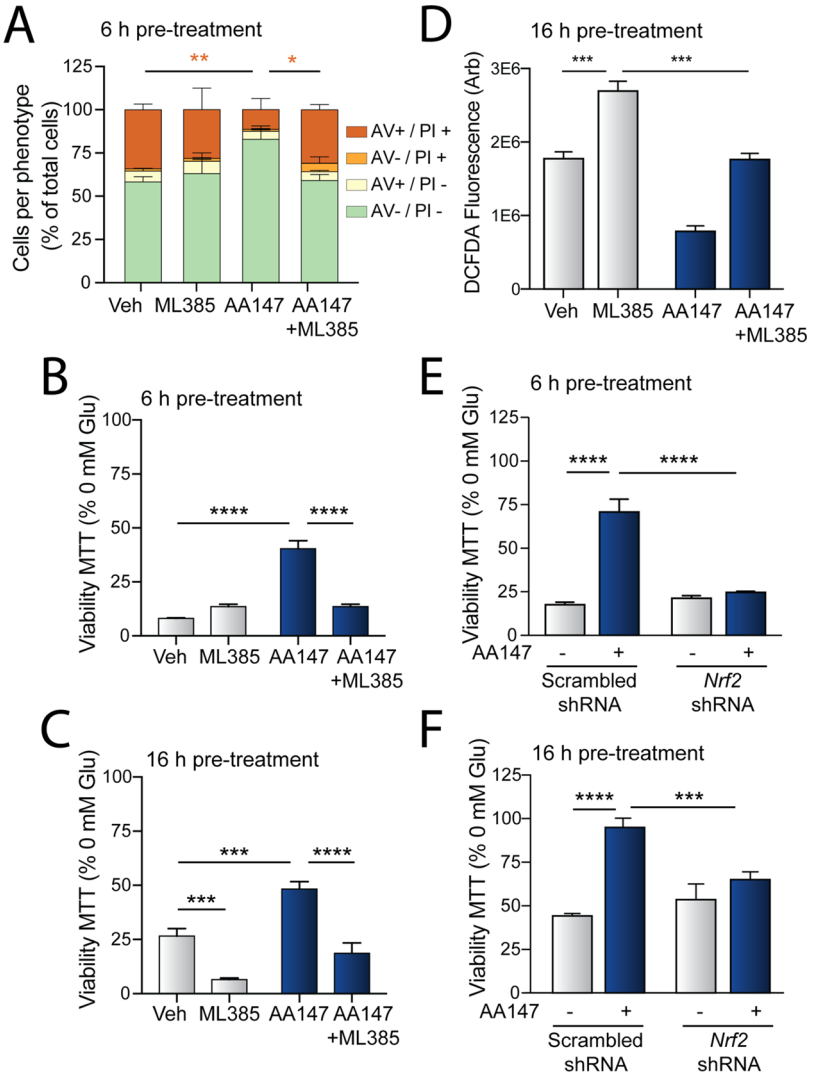

Figure 6. AA147-induced protection from glutamate toxicity is attenuated by NRF2 inhibition. (A) Quantification of the percent of HT22 cells pretreated with AA147 for 6 h and then challenged with glutamate (5 mM) for 24 h stained with Annexin V (AV) and/or propidium iodide (PI). Error bars show SEM for $n = 3$ replicates. *$p < 0.05$ and **$p < 0.01$ for ordinary one-way ANOVA with Tukey correction for multiple comparisons. (B, C) Viability, measured by MTT, of HT22 cells pretreated with AA147 (10 μM) for 6 h (B) or 16 h (C) in the presence or absence of the NRF2 inhibitor ML385 (5 μM) and then challenged with glutamate (5 mM) for 24 h. Viability is reported as percent relative to vehicle. ***$p < 0.001$ and ****$p < 0.0001$ for two-way ANOVA relative to vehicle with Tukey correction for multiple comparisons between conditions. (D) Mean CM-H2DCFDA fluorescence of HT22 cells pretreated with AA147 (10 μM) and/or ML385 (5 μM) for 16 h and then challenged with glutamate (5 mM) for 8 h, as indicated. Error bars show SEM for $n = 3$ replicates. ***$p < 0.001$ for two-way ANOVA with Tukey correction for multiple comparisons between conditions. (E, F) Viability, measured by MTT, of HT22 cells pretreated with AA147 (10 μM) for 6 h (E) or 16 h (F) in HT22 cells expressing scrambled or *Nrf2* shRNA challenged with glutamate (5 mM) for 24 h. Viability is shown as a percent cell with respective treatments in the absence of glutamate. ***$p < 0.001$ and ****$p < 0.0001$ for two-way ANOVA relative to vehicle with Tukey correction for multiple comparisons.

glutamate-induced toxicity.[37,38] Many of the antioxidant genes induced by AA147 are known transcriptional targets of NRF2 (e.g., *Nqo1*, *Gsta4*).[31−33] Thus, we sought to determine whether AA147 was activating NRF2 in HT22 cells. Initially, we showed that AA147 increased the expression of an NRF2-selective ARE-LUC reporter in HT22 cells (Figure 4C).[35] AA147 activated this ARE-LUC reporter with an EC_{50} of 3.9 μM, which is nearly identical to that observed for compound-dependent activation of the ATF6-selective ERSE-LUC reporter (Figure S1A). Next, we used qPCR to confirm that AA147 induced the expression of NRF2 target genes including *Nqo1* and *Gsta4* in HT22 cells (Figures 4 and S4C). Cotreatment with the NRF2 inhibitor ML385, which inhibits NRF2 binding to DNA,[39] reduced AA147-dependent *Nqo1* and *Gsta4* induction (Figures 4D and S4C). Similar results were observed by immunoblotting (Figure S4D). Further, shRNA depletion of *Nrf2* blocked the AA147-dependent induction of *Gsta4*, but not *BiP*, in HT22 cells treated with AA147 for 6 h (Figure S4E,F). This indicates that AA147 induces the expression of NRF2 target genes in HT22 cells through an NRF2-dependent mechanism.

Previous transcriptional profiling of AA147-treated HEK293T cells did not show the increased expression of NRF2 target genes, suggesting that the observed increase in their expression could be cell-type-specific. To further probe this, we monitored the expression of the ATF6 target gene *BiP* and the NRF2 target gene *Nqo1* in two neuronal-derived cell lines (HT22 and IMR32), as well as three non-neuronal-

https://doi.org/10.1021/acschembio.1c00810
ACS Chem. Biol. 2021, 16, 2852−2863

derived cell lines (HEK293T, U2OS, and HeLa) treated with AA147 for increasing times (Figure S4G–K). AA147 induced the expression of the ATF6 target gene *BiP* in all cells following 4 h treatment. However, the increased expression of the NRF2 target gene *Nqo*1 was only observed in the neuronal-derived HT22 and IMR32 cells beginning at 4 h. We further showed the ability of AA147 to induce the expression of the NRF2 target gene *Nqo*1 in mouse primary cortical neurons treated with AA147 for 6 h (Figure S4L). This indicated that AA147-dependent NRF2 activation is cell-type specific, with some selectivity for neuronal-derived cell lines. Interestingly, the amount of $AA147^{alk}$ protein labeling across different cell lines generally correlates with the expression of ATF6 and NRF2 target genes observed in AA147-treated cells (Figure S4M). This indicates that the variability in response between cells could be dependent on the extent of metabolic activation and/or protein labeling. In combination with the existing literature,[14,15,24,27,28] these results suggest that AA147 induces ATF6 activity broadly across cell types, whereas AA147-dependent NRF2 activation is only observed in select cell types including neuronal-derived HT22 and IMR32 cells.

AA147 Covalently Modifies KEAP1 to Promote NRF2 Activation in HT22 Cells. NRF2 activity is primarily regulated through its interaction with the redox sensor E3 ligase protein KEAP1 (Figure 5A).[39,40] In the absence of oxidative stress, KEAP1 promotes the ubiquitination of NRF2 leading to its inactivation by degradation.[40] In response to oxidative stress, sensor cysteine residues on KEAP1, such as Cys151, are covalently modified by electrophiles or oxidants, reducing KEAP1-dependent ubiquitination of NRF2 and stabilizing it to promote its transcriptional activity.[40,41] Since AA147 can be metabolically activated to a reactive electrophile that can covalently modify proteins, we predicted that AA147 activates NRF2 in HT22 cells through a mechanism involving metabolic activation and covalent modification of KEAP1.

Consistent with this, cotreatment with AA147 and either resveratrol or β-mercaptoethanol, conditions that reduce $AA147^{alk}$ covalent protein modification (Figure 2C), inhibits AA147-dependent activation of the NRF2-selective ARE-LUC reporter and the ATF6-selective ERSE-LUC reporter in HT22 cells (Figure S5A). Further, AA147 analogues lacking the 2-amino-*p*-cresol moiety in the AA147 A-ring showed no activation of ARE-LUC reporter, while B-ring analogues retained this activity (Figure 5B). This structure–activity relationship is similar to that observed for the compound-dependent activation of the ATF6-selective ERSE-LUC reporter (Figure S5B). Finally, $AA147^{N\text{-methyl}}$, an analogue that disfavors the formation of the AA147-QI (Figure S2G), does not significantly induce the expression of either the ARE-LUC or ERSE-LUC reporters in HT22 cells (Figure S5C). Collectively, these results support a model whereby AA147 activates NRF2 through a mechanism involving metabolic activation and covalent protein modification (Figure 2B).

Next, we monitored the potential for AA147 to covalently modify KEAP1. We expressed FLAG-tagged KEAP1 ($KEAP1^{FT}$) in HEK293 cells treated with or without $AA147^{alk}$. We then labeled $AA147^{alk}$ with rhodamine-azide using click chemistry and monitored the population of rhodamine-labeled and total immunoprecipitated $KEAP1^{FT}$ by sodium dodecyl sulfate-polyacrylamide gel electrophoresis (SDS-PAGE) using rhodamine fluorescence and immunoblotting, respectively. We observed dose-dependent increases in $KEAP1^{FT}$ labeling with AA147, confirming that our compound covalently targets KEAP1 (Figure S5D). Mutating the KEAP1 sensor cysteine 151 to serine (C151S) showed reduced labeling with $AA147^{alk}$, indicating that AA147 modifies this redox-sensing cysteine involved in regulating NRF2 activity (Figures 5C and S5D). These results demonstrate that AA147 is metabolically activated to a reactive electrophile that can modify KEAP1 at the sensor cysteine C151.

NRF2 Inhibition Attenuates AA147-Dependent Protection against Glutamate-Induced Toxicity. Upregulation of the NRF2 transcriptional activity protects against glutamate toxicity in HT22 cells.[13,38,42] Therefore, we asked whether the protection afforded by AA147 in this model was mediated by NRF2 activity. To test this, we co-pre-treated HT22 cells with AA147 and the NRF2 inhibitor ML385 for 6 h prior to the addition of glutamate. After a 24 h glutamate challenge, we then monitored cell death by Annexin V and PI staining. Cotreatment with ML385 significantly inhibited AA147-dependent reductions in glutamate-induced cell death (Figures 6A and S6A). Similar results were observed using a viability assay in cells treated with AA147 and ML385 at both 6 h (Figure 6B) and 16 h (Figure 6C). HT22 cells treated with ML385 for 16 h did show reductions in viability, which was modestly improved with AA147 treatment. This could reflect a modest role for AA147-dependent ATF6 activation protection observed under these conditions. Consistent with this, HT22 cells cotreated with either the ATF6 inhibitor S1Pi (Figure S6B) or the NRF2 inhibitor ML385 (Figure 6D) both attenuated AA147-dependent reductions of ROS in glutamate-treated HT22 cells treated for 16 h. This suggests that both ATF6 and NRF2 activation can contribute to reductions in ROS observed under these conditions.

We next shRNA-depleted *Nrf*2 in HT22 cells to further define the dependence of the observed AA147-dependent protection against glutamate toxicity on NRF2 activity (Figure S4E). AA147 did not improve viability in glutamate-treated HT22 cells shRNA-depleted of *Nrf*2, either at 6 h (Figure 6E) or 16 h (Figure 6F). This indicates that NRF2 is required for the AA147-dependent protection observed at both of these time points. We further defined the dependence of AA147-mediated protection against glutamate toxicity in HT22 using the alternative NRF2 activator CBR-470-1—a compound that activates NRF2 through a mechanism involving the inhibition of the glycolytic enzyme PGK1.[43] We confirmed that CBR-470-1 protects HT22 against glutamate-induced toxicity, showing similar levels of protection to that observed for AA147 (Figure S6C–E). However, pretreatment with both AA147 and CBR-470-1 for 16 h did not show further increases in protection, suggesting that these two NRF2 activators protect HT22 cells against glutamate toxicity through a similar mechanism (Figure S6E). Combined, these results indicate that AA147-dependent NRF2 activation is the primary mechanism of protection against glutamate toxicity in these cells.

Concluding Remarks. Previous results showed that the proteostasis regulator compound AA147 protects against oxidative damage through the activation of the ATF6 signaling arm of the UPR.[14,15] Here, we demonstrate that AA147 protects against glutamate-induced oxidative toxicity in neuronal-derived HT22 cells primarily through a mechanism involving the activation of the NRF2-regulated oxidative stress response. Our results indicate that AA147-dependent activation of ATF6 and NRF2 shares a similar mechanism of activation involving compound oxidation to a reactive

https://doi.org/10.1021/acschembio.1c00810
ACS Chem. Biol. 2021, 16, 2852–2863

electrophile and covalent modification of protein substrates.[20] However, unlike ATF6 activation, which involves the AA147-dependent modification of PDIs,[16,20] the AA147-dependent activation of NRF2 involves compound-dependent modification of KEAP1. This demonstrates that protective NRF2 signaling can be activated in neurons using metabolically activated compounds such as AA147. Further, our results indicate that AA147 can promote protection against oxidative insults in neuronal cells through the activation of two distinct stress-responsive signaling pathways, the ATF6 arm of the UPR[16] and the NRF2 oxidative stress response (described herein). These results highlight the broad potential for this compound to mitigate oxidative damage in etiologically diverse diseases, including many neurodegenerative disorders.

MATERIALS AND METHODS

Compounds, Antibodies, and Plasmids. AA147 and associated analogues were reported previously and obtained from the Kelly Lab at Scripps Research.[20] AA147 and related analogues were suspended in dimethyl sulfoxide (DMSO).[20] Cells were treated with 10 μM of these compounds for all experiments except where otherwise stated. PF429242 (Sigma-Aldrich; cat SML0667) was resuspended in water and administered at 10 μM. CP7 was obtained from the Walter Lab at UCSF, resuspended in DMSO, and administered at 5 μM. ML385 (Cayman Chemicals; cat. 21114) was resuspended in DMSO and administered at 5 μM. Glutamate stocks were prepared using glutamic acid (Acros Organics; cat. AC156211000) resuspended in water and the pH was adjusted to 7.5. Equivalent water volume was used as control for all 0 mM glutamate treatments. The following antibodies were purchased and utilized in this study as indicated: NQO1 (1:1000; Abcam cat. ab80588), KDEL (1:1000; Enzo cat. ADI-SPA-827-F), and tubulin (1:2000; Sigma-Aldrich T6074). The ERSE-LUC and ARE-LUC plasmids were previously described.[15,43] For viral transfection, the following plasmids were used: REV (pRSV-rev; Addgene cat. 12253), RRE (pMDL-RRE; Addgene cat. 12251), and VSV-G (pMD2.G; Addgene cat. 12259). *ATF6* and *NRF2* shRNAs in pLKO.1 vectors were obtained from La Jolla Institute for Allergy and Immunology (LJI). The specific target sequences for viral plasmid of these shRNAs are below:

ATF6-1-TRCN0000008447 CCGGCGAAGGGATCATCTGCTATTACTCGAGTAATAGCAGATGATCCCTTCGTTTTT

ATF6-TRCN0000008448 CCGGGCCATCATCATTCAGACACTACTCGAGTAGTGTCTGAATGATGATGGCTTTTT

NRF2- TRCN0000007555 CCGGGCTCCTACTGTGATGTGAAATCTCGAGATTTCACATCACAGTAGGAGCTTTTT

Cell Culture Maintenance and shRNA Depletion. HT22 cells were a kind gift from Pamela Maher at the Salk Institute. HT22 cells were split when 70% confluent and discarded after 10 passages. During experimental testing, HT22 cells were plated at a density of 5 × 10^3 per well for a 96-well plate or equivalent density for larger plates. All cells were routinely tested for mycoplasma and incubated in high glucose Dulbecco's modified Eagle medium (DMEM) supplemented with 10% fetal bovine serum (FBS), glutamate, and penicillin/streptomycin at 37 °C and 5% CO_2. For shRNA depletion, viruses expressing specific shRNAs were prepared as previously described.[20] Briefly, one 10 cm dish of HEK293T cells per shRNA was transiently transfected with 8 μg shRNA construct, 4 μg REV (pRSV-rev), 4 μg RRE (pMDL-RRE), and 4 μg VSV-G (pMD2.G). Transfection reagents were removed after a 24 h incubation, followed by a 24 h incubation for viral production in fresh media. A 1:1 ratio of virus-containing media and fresh media was added to HT22 cells for 24 h. Transfected cells were puromycin-selected (5 μg/L) (Sigma-Aldrich; cat P8833) for 7 days. Knockdown was confirmed by real-time quantitative polymerase chain reaction (RT-qPCR).

Primary Neuronal Culture. Primary cortical neurons were isolated from C57BL/6J P1 mouse pups. Isolated cortices were suspended in cold dissection media (1× HBSS w/o Ca and Mg, 2% HEPES, 1× sodium pyruvate, 1% glucose solution, and. 02% gentamicin). Isolated cortices were incubated with papain (0.2 μg/mL final) for 20 min at 37 °C. Following incubation, cortices were mechanically disrupted and filtered using a 40 μm cell strainer. Viability of isolated neurons was measured using trypan blue nitrogen countess II cell counter before plating. Cells in 96-well plates were plated on PDK-coated plastic plates in neurobasal A media with 2% B27 supplement at a density of 50K cells per well. Glial inhibitors (10 μM of 5-fluoro-2′-deoxyuridine and 10 μM uridine) were added at DIV4 with a 50% media change. These were included with subsequent 50% media changes, which were performed every 3−4 days following plating. Morphology was evaluated prior to each media change and immediately prior to experiments, which were performed at DIV27.

Viability Assay. Pretreatments were administered as described, and glutamate was added for 24 h prior to assessing viability using Cell-Titer Glo reagent (Promega; cat. PRG7572) or 3-(4,5-dimethylthiazol-2-yl)-2,5-diphenyltetrazolium bromide (MTT) (Life Sciences; cat. M6494). Cell-Titer Glo was performed following the manufacturer's protocol. MTT viability assays were performed as described elsewhere.[44] Briefly, MTT was resuspended in Dulbecco's phosphate-buffered saline (DPBS; Life Tech; cat. 14190235) at a concentration of 5 mg/mL and sterile-filtered prior to use. Cells were treated in 100 μL of media. Ten microliters of MTT solution was added to media and incubated at 37 °C for 4 h. The reaction was halted by adding 100 μL of a stop solution consisting of 10% SDS with 10 mM HCl. Cells were allowed to completely lyse by an overnight incubation at 37 °C. Absorbance was measured using a SPECTRAmax PLUS 384 (Molecular Devices) plate reader at OD570 with an OD630 reference.

Propidium Iodide (PI) and Annexin V Staining. PI/Annexin V staining was performed on HT22 cells treated as indicated. Cells were challenged with glutamate for 24 h. We then harvested the cells from the plate, washed with DPBS, and resuspended in 50 μL of 1× Annexin V binding buffer (BD Biosciences; cat. 556454). Cells were incubated in the dark at RT with 3 μL propidium iodide (Miltenyi Biotech; cat. 130-093-233) and 3 μL FITC-Annexin V (BD Biosciences; cat. 556419) for 20 min and then diluted with 100 μL binding buffer. Unstained and single-channel controls were used for compensation calculations for each experiment. Flow cytometry was performed on a NovoCyte 3000 (Acea); PI was detected at ex. 488 nm, em. 615/20 nm and FITC-Annexin V using ex. 488 nm, em. 530/30 nm channel. Analysis and gating were performed using FlowJo software (BD Biosciences, San Diego).

Quantification of ROS by DCFDA Fluorescence. Cells were plated in 24-well clear tissue culture-treated plates (Genesee Scientific, San Diego), and compounds were pretreated as stated for 16 h. Glutamate was added for 8 h. Following glutamate incubation, cells were harvested and then washed and resuspended in DPBS. CM-H2DCFDA (Invitrogen; cat. C6827) was freshly dissolved in DMSO. Cells were incubated in 5 μM CM-H2DCFDA for 30 min and immediately run on a NovoCyte 3000 (Acea) using ex. 488 nm, em. 530/30 nm channel. Cytometric analysis was performed using FlowJo software (BD Biosciences, San Diego).

Luciferase Assays. Cells were seeded at a density of 3,500 cells per well into flat white 384-well plates (Corning). The following day, cells were transfected with p-TI-ARE-LUC[43] or pcDNA3.1-ERSE-LUC[15] plasmids (100 ng/well) using polyethyleneimine (PEI) at a ratio of 2:1 (PEI/DNA). Media was changed 16 h later to remove PEI. Cells were treated as indicated for 16 h and then lysed by the addition of Bright-Glo (Promega). Samples were dark-adapted for 20 min to stabilize signals. Luminescence was then measured in an Infinite F200 PRO plate reader (Tecan) and corrected for background signal.

Synthesis of *N*-(2-Hydroxy-5-methylphenyl)-*N*-methyl-3-phenylpropanamide (AA147$^{N\text{-methyl}}$). To a stirring solution of sodium hydride (60% mineral oil dispersion, 12 mg, 0.3 mmol, 1.5 equiv) in 5 mL anhydrous tetrahydrofuran (THF) at 0 °C was added methoxymethyl ether derivative of AA147 (**1**) (60 mg, 0.2 mmol, 1 equiv).[1] The reaction was stirred for 10 min. Methyl iodide (56 mg, 0.4 mmol, 2 equiv) was added slowly, and the reaction was allowed to

https://doi.org/10.1021/acschembio.1c00810
ACS Chem. Biol. 2021, 16, 2852−2863

Table 1. Forward and Reverse Primers

gene	forward primer	reverse primer
mRiboP	5′-TGTCATCGCTCAGGGTGTTG-3′	5′-AAGCCAAATCCCATGTCGTC-3′
mBiP	5′-GTCCAGGCTGGTGTCCTCTC-3′	5′-GATTATCGGAAGCCGTGGAG-3′
mGsta4	5′-CCCCCAAGGAAAAAGAGGAG3′	5′-TGGATGTCTGCCCAACTGAG-3′
mNqo1	5′-TCTCTGGCCGATTCAGAGTG-3′	5′-CTCCCAGACGGTTTCCAGAC-3′
mNrf2	5′-CAGGCCCAGTCCCTCAATAG-3′	5′-TCAGCCAGCTGCTTGTTTTC-3′
mAtf6	5′-GGAGTCGACGTTGTTTGCTG-3′	5′-GGTCTGACTCCCAAGGCATC-3′

stir overnight at room temperature. The reaction was then partitioned between 1 N HCl and EtOAc, and the separated organic layer was washed with water, dried over $MgSO_4$, and concentrated under reduced pressure. To the resulting residue dissolved in 1 mL THF was added 100 μL of 12.1 N HCl and let stir overnight. The reaction was diluted in EtOAc and washed with saturated sodium bicarbonate. The organic layer was washed with brine, dried over $MgSO_4$, and concentrated. Purification of the crude residue by column chromatography afforded the title compound as a light brown solid (13.2 mg, 25% yield). ^{1}H NMR (400 MHz, DMSO) δ 7.26−7.19 (m, 2H), 7.17−7.08 (m, 1H), 7.11−7.01 (m, 2H), 6.96 (ddd, J = 8.2, 2.2, 0.8 Hz, 1H), 6.86−6.78 (m, 2H), 3.03 (s, 3H), 2.75 (t, 2H), 2.33−2.18 (m, 2H), 2.17 (s, 3H). ^{13}C NMR (126 MHz, DMSO) δ 171.3, 150.5, 141.4, 130.2, 129.4, 129.1, 128.4, 128.2, 128.1, 125.8, 116.4, 35.4, 34.9, 30.8, 19.8. LRMS (m/z) $[M + H]^+$ calculated for $C_{17}H_{19}NO_2$ 269.14; found 269.1.

KEAP1 Modification. Cells were transiently transfected with FLAG-KEAP1 C151S or WT construct. The following day, media was changed to remove the transfection agent. The following day, cells were incubated with 10 μM AA147^{alk} or otherwise as described for 1 h. Cells were washed with DPBS and lysed in RIPA followed by sonication. The lysate was incubated with M2-FLAG beads overnight. Beads were washed three times, and FLAG-tagged proteins were eluted using 3× FLAG peptide (Sigma-Aldrich; cat. F4799). Rhodamine-azide labeling reactions were performed using 1.7 mM TBTA, 50 mM $CuSO_4$, 5 mM azide, and 50 mM tris(2-carboxyethyl)phosphine (TCEP). The protein was purified using MeOH precipitation and run on a 4−12% Bis−Tris polyacrylamide gel. The eluate was resuspended in Laemmli sample buffer, and proteins were resolved on a 4−12% Bis−Tris polyacrylamide gel and immunoblotted using 1:1000 M2-FLAG antibody (Sigma-Aldrich; cat. F1804).

Quantitative PCR (qPCR). HT22 cells were treated with 10 μM AA147 or DMSO vehicle for either 6 or 16 h. Cells were rinsed with PBS, lysed, and total RNA was collected using the QuickRNA mini kit (Zymo) according to the manufacturer's instructions. The relative quantification of mRNA was calculated using qPCR with reverse transcription (RT-qPCR). RNA yield was quantified using Nanodrop. cDNA was generated from 300 ng of RNA using High-Capacity cDNA Reverse Transcription Kit (Advanced Biosystems; cat. 4368814). qPCR reactions were prepared using Power SYBR Green PCR Master Mix (Applied Biosystems; cat. 4367659), and primers (Table 1) were obtained from Integrated DNA Technologies. Amplification reactions were run in an ABI 7900HT Fast Real Time PCR machine with an initial melting period of 95 °C for 5 min and then 45 cycles of 10 s at 95 °C, 30 s at 60 °C.

Immunoblotting. Cell lysates were prepared as previously described.[45] Briefly, cells were lysed in RIPA buffer (50 mM Tris, pH 7.5, 150 mM NaCl, 0.1% SDS, 1% Triton X-100, 0.5% deoxycholate, and protease inhibitor cocktail (Roche)). The total protein concentration in cellular lysates was normalized using the Bio-Rad protein assay. Lysates were then denatured with 1 × Laemmli buffer + 100 mM dithiothreitol (DTT) and boiled before being separated by SDS-PAGE. Samples were transferred onto nitrocellulose membranes (Bio-Rad). Membranes were then incubated overnight at 4 °C with primary antibodies diluted at 1:1000. Membranes were washed in TBST, incubated with the species-appropriate IR-Dye conjugated secondary antibodies, and analyzed using the Odyssey Infrared Imaging System (LI-COR Biosciences). Quantification was carried out with LI-COR Image Studio software.

RNA Sequencing. HT22 cells were treated for 16 h with 10 μM AA147 or vehicle. Cells were rinsed with DPBS, lysed, and total RNA was collected using the QuickRNA mini kit (Zymo) according to the manufacturer's instructions. Transcriptional profiling using whole transcriptome RNA sequencing was conducted via BGI Americas on the BGI Proprietary platform with three biological replicates for each condition. All samples were sequenced to a minimum depth of 27 M PE 100 bp reads. Alignment of reads was performed using DNAstar Lasergene SeqManPro to the mouse genome GRCm39 assembly. Aligned reads were imported into ArrayStar 12.2 with QSeq (DNAStar Inc.) to quantify the gene expression levels. Differential expression analysis and statistical significance calculations between different conditions were assessed using DESeq. 2 in R compared to vehicle-treated cells. The complete RNA-seq data is deposited in gene expression omnibus (GEO) as GSE178964.

Code Availability. Code for the standard open-source DESeq. 2 differential gene expression RNA-seq analysis used in R statistical software is available from the corresponding author upon reasonable request.

Statistical Methods. All statistical analyses were performed using Prism 9 (GraphPad, San Diego, CA) as described. The number of replicates and independent experiments for each figure panel are clearly stated in the figure legends. One-way ANOVA statistical tests were used to detect statistically significant differences between the means of three or more treatments with post hoc testing to define specific statistical relationships. Two-way ANOVA statistical tests were used to detect statistically significant basal changes in viability or in viability following a glutamate challenge in HT22 cells treated with vehicle AA147 in the presence or absence of a pathway signaling inhibitor (e.g., S1Pi, shRNA). The appropriate multiple testing correction for post hoc analyses was performed as noted for each experiment. EC_{50} calculations were performed using log(agonist) vs response variable slope four-parameter nonlinear function with least-squares fit.

■ ASSOCIATED CONTENT

Supporting Information

The Supporting Information is available free of charge at https://pubs.acs.org/doi/10.1021/acschembio.1c00810.

Additional viability assays, gene expression data, representative flow cytometry plots, representative gels, synthesis and validation information for AA147$^{N\text{-methyl}}$, and figure legends for Figures S1−S6 and supplemental table legends for Tables S1 and S2 (PDF)

RNAseq of HT22 cells treated with AA147 for 16 h (Table S1) (XLSX)

Geneset-based stress-signaling pathway profiling of HT22 cells treated with AA147 for 16 h (Table S2) (XLSX)

■ AUTHOR INFORMATION

Corresponding Author

R. Luke Wiseman − *Department of Molecular Medicine, The Scripps Research Institute, La Jolla, California 92037, United*

https://doi.org/10.1021/acschembio.1c00810
ACS Chem. Biol. 2021, 16, 2852−2863

States; orcid.org/0000-0001-9287-6840; Email: wiseman@scripps.edu

Authors

Jessica D. Rosarda − *Department of Molecular Medicine, The Scripps Research Institute, La Jolla, California 92037, United States*

Kelsey R. Baron − *Department of Molecular Medicine, The Scripps Research Institute, La Jolla, California 92037, United States*

Kayla Nutsch − *Department of Chemistry, The Scripps Research Institute, La Jolla, California 92037, United States*

Gabriel M. Kline − *Department of Chemistry and The Skaggs Institute for Chemical Biology, The Scripps Research Institute, La Jolla, California 92037, United States*

Caroline Stanton − *Department of Molecular Medicine, The Scripps Research Institute, La Jolla, California 92037, United States; Department of Chemistry, The Scripps Research Institute, La Jolla, California 92037, United States*

Jeffery W. Kelly − *Department of Chemistry and The Skaggs Institute for Chemical Biology, The Scripps Research Institute, La Jolla, California 92037, United States;* orcid.org/0000-0001-8943-3395

Michael J. Bollong − *Department of Chemistry, The Scripps Research Institute, La Jolla, California 92037, United States;* orcid.org/0000-0001-9439-1476

Complete contact information is available at: https://pubs.acs.org/10.1021/acschembio.1c00810

Notes

The authors declare the following competing financial interest(s): JWK declares that he is a board member and shareholder of Proteostasis Therapeutics Inc., Protego BioPharma, and Yumanity. RLW is a stockholder and scientific advisory board member of Protego Biopharma who have licensed this compound for translational development. JWK and RLW are also inventors on patents describing AA147. All other authors declare no conflicts.

■ ACKNOWLEDGMENTS

The authors thank P. Maher (Salk Institute) for generously providing HT22 cells and L. Ibrahim and D. Rosen at Scripps Research for fruitful discussions and experimental support related to the work described herein. The authors would also like to thank E. Powers and M. Petrascheck for critical reading of this manuscript. This work was supported by the NIH (AG095892 and DK107604 to R.L.W.).

■ ABBREVIATIONS

NRF2, nuclear factor erythroid 2-related factor 2; ATF6, activating transcription factor 6; UPR, unfolded protein response; ER, endoplasmic reticulum; S1P, site 1 protease; ERSE, ER-stress-responsive element; ARE, antioxidant response element

■ REFERENCES

(1) Bano, D.; Young, K. W.; Guerin, C. J.; Lefeuvre, R.; Rothwell, N. J.; Naldini, L.; Rizzuto, R.; Carafoli, E.; Nicotera, P. Cleavage of the plasma membrane Na+/Ca2+ exchanger in excitotoxicity. *Cell* **2005**, *120*, 275−285.

(2) Armada-Moreira, A.; Gomes, J. I.; Pina, C. C.; Savchak, O. K.; Gonçalves-Ribeiro, J.; Rei, N.; Pinto, S.; Morais, T. P.; Martins, R. S.; Ribeiro, F. F.; et al. Going the Extra (Synaptic) Mile: Excitotoxicity as the Road Toward Neurodegenerative Diseases. *Front. Cell. Neurosci.* **2020**, *14*, No. 90.

(3) Dirnagl, U.; Iadecola, C.; Moskowitz, M. A. Pathobiology of ischaemic stroke: an integrated view. *Trends Neurosci.* **1999**, *22*, 391−397.

(4) Ankarcrona, M.; Dypbukt, J. M.; Bonfoco, E.; Zhivotovsky, B.; Orrenius, S.; Lipton, S. A.; Nicotera, P. Glutamate-induced neuronal death: a succession of necrosis or apoptosis depending on mitochondrial function. *Neuron* **1995**, *15*, 961−973.

(5) Kritis, A. A.; Stamoula, E. G.; Paniskaki, K. A.; Vavilis, T. D. Researching glutamate-induced cytotoxicity in different cell lines: a comparative/collective analysis/study. *Front. Cell. Neurosci.* **2015**, *9*, No. 91.

(6) Maher, P.; Davis, J. B. The role of monoamine metabolism in oxidative glutamate toxicity. *J. Neurosci.* **1996**, *16*, 6394−6401.

(7) Soria, F. N.; Perez-Samartin, A.; Martin, A.; Gona, K. B.; Llop, J.; Szczupak, B.; Chara, J. C.; Matute, C.; Domercq, M. Extrasynaptic glutamate release through cystine/glutamate antiporter contributes to ischemic damage. *J. Clin. Invest.* **2014**, *124*, 3645−3655.

(8) Davis, J. B.; Maher, P. Protein kinase C activation inhibits glutamate-induced cytotoxicity in a neuronal cell line. *Brain Res.* **1994**, *652*, 169−173.

(9) Long, J. M.; Holtzman, D. M. Alzheimer Disease: An Update on Pathobiology and Treatment Strategies. *Cell* **2019**, *179*, 312−339.

(10) Berthier, M. L.; Green, C.; Lara, J. P.; Higueras, C.; Barbancho, M. A.; Dávila, G.; Pulvermüller, F. Memantine and constraint-induced aphasia therapy in chronic poststroke aphasia. *Ann. Neurol.* **2009**, *65*, 577−585.

(11) Trotman, M.; Vermehren, P.; Gibson, C. L.; Fern, R. The dichotomy of memantine treatment for ischemic stroke: dose-dependent protective and detrimental effects. *J. Cereb. Blood Flow Metab.* **2015**, *35*, 230−239.

(12) Maher, P.; Currais, A.; Schubert, D. Using the Oxytosis/Ferroptosis Pathway to Understand and Treat Age-Associated Neurodegenerative Diseases. *Cell Chem. Biol.* **2020**, *27*, 1456−1471.

(13) Lewerenz, J.; Maher, P. Control of redox state and redox signaling by neural antioxidant systems. *Antioxid. Redox Signaling* **2011**, *14*, 1449−1465.

(14) Blackwood, E. A.; Azizi, K.; Thuerauf, D. J.; Paxman, R. J.; Plate, L.; Kelly, J. W.; Wiseman, R. L.; Glembotski, C. C. Pharmacologic ATF6 activation confers global protection in widespread disease models by reprograming cellular proteostasis. *Nat. Commun.* **2019**, *10*, No. 187.

(15) Plate, L.; Cooley, C. B.; Chen, J. J.; Paxman, R. J.; Gallagher, C. M.; Madoux, F.; Genereux, J. C.; Dobbs, W.; Garza, D.; Spicer, T. P.; et al. Small molecule proteostasis regulators that reprogram the ER to reduce extracellular protein aggregation. *eLife* **2016**, *5*, No. 15550.

(16) Glembotski, C. C.; Rosarda, J. D.; Wiseman, R. L. Proteostasis and Beyond: ATF6 in Ischemic Disease. *Trends Mol. Med.* **2019**, *25*, 538−550.

(17) Ye, J.; Rawson, R. B.; Komuro, R.; Chen, X.; Davé, U. P.; Prywes, R.; Brown, M. S.; Goldstein, J. L. ER Stress Induces Cleavage of Membrane-Bound ATF6 by the Same Proteases that Process SREBPs. *Mol. Cell* **2000**, *6*, 1355−1364.

(18) Shoulders, M. D.; Ryno, L. M.; Genereux, J. C.; Moresco, J. J.; Tu, P. G.; Wu, C.; Yates, J. R., 3rd; Su, A. I.; Kelly, J. W.; Wiseman, R. L. Stress-independent activation of XBP1s and/or ATF6 reveals three functionally diverse ER proteostasis environments. *Cell Rep.* **2013**, *3*, 1279−1292.

(19) Adachi, Y.; Yamamoto, K.; Okada, T.; Yoshida, H.; Harada, A.; Mori, K. ATF6 is a transcription factor specializing in the regulation of quality control proteins in the endoplasmic reticulum. *Cell Struct. Funct.* **2008**, *33*, 75−89.

(20) Paxman, R.; Plate, L.; Blackwood, E. A.; Glembotski, C.; Powers, E. T.; Wiseman, R. L.; Kelly, J. W. Pharmacologic ATF6 activating compounds are metabolically activated to selectively modify endoplasmic reticulum proteins. *eLife* **2018**, *7*, No. e37168.

(21) Wang, S.; Kaufman, R. J. The impact of the unfolded protein response on human disease. *J. Cell Biol.* **2012**, *197*, 857−867.

(22) Martindale, J. J.; Fernandez, R.; Thuerauf, D.; Whittaker, R.; Gude, N.; Sussman, M. A.; Glembotski, C. C. Endoplasmic Reticulum Stress Gene Induction and Protection From Ischemia/Reperfusion Injury in the Hearts of Transgenic Mice With a Tamoxifen-Regulated Form of ATF6. *Circ. Res.* **2006**, *98*, 1186−1193.
(23) Chen John, J.; Genereux Joseph, C.; Qu, S.; Hulleman John, D.; Shoulders Matthew, D.; Wiseman, R. L. ATF6 Activation Reduces the Secretion and Extracellular Aggregation of Destabilized Variants of an Amyloidogenic Protein. *Chem. Biol.* **2014**, *21*, 1564−1574.
(24) Kroeger, H.; Grimsey, N.; Paxman, R.; Chiang, W. C.; Plate, L.; Jones, Y.; Shaw, P. X.; Trejo, J.; Tsang, S. H.; Powers, E.; et al. The unfolded protein response regulator ATF6 promotes mesodermal differentiation. *Sci. Signaling* **2018**, *11*, No. 5785.
(25) Shen, Y.; Li, R.; Yu, S.; Zhao, Q.; Wang, Z.; Sheng, H.; Yang, W. Activation of the ATF6 (Activating Transcription Factor 6) Signaling Pathway in Neurons Improves Outcome After Cardiac Arrest in Mice. *J. Am. Heart Assoc.* **2021**, *10*, No. e020216.
(26) Kroeger, H.; Grandjean, J. M. D.; Chiang, W.-CJ.; Bindels, D. D.; Mastey, R.; Okalova, J.; Nguyen, A.; Powers, E. T.; Kelly, J. W.; Grimsey, N. J.; et al. ATF6 is essential for human cone photoreceptor development. *Proc. Natl. Acad. Sci. U.S.A.* **2021**, *118*, No. e2103196118.
(27) Rius, B.; Mesgarzadeh, J. S.; Romine, I. C.; Paxman, R. J.; Kelly, J. W.; Wiseman, R. L. Pharmacologic targeting of plasma cell endoplasmic reticulum proteostasis to reduce amyloidogenic light chain secretion. *Blood Adv.* **2021**, *5*, 1037−1049.
(28) Almasy, K. M.; Davies, J. P.; Lisy, S. M.; Tirgar, R.; Tran, S. C.; Plate, L. Small-molecule endoplasmic reticulum proteostasis regulator acts as a broad-spectrum inhibitor of dengue and Zika virus infections. *Proc. Natl. Acad. Sci. U.S.A.* **2021**, *118*, No. e2012209118.
(29) Fukui, M.; Song, J. H.; Choi, J.; Choi, H. J.; Zhu, B. T. Mechanism of glutamate-induced neurotoxicity in HT22 mouse hippocampal cells. *Eur. J. Pharmacol.* **2009**, *617*, 1−11.
(30) Hawkins, J. L.; Robbins, M. D.; Warren, L. C.; Xia, D.; Petras, S. F.; Valentine, J. J.; Varghese, A. H.; Wang, I. K.; Subashi, T. A.; Shelly, L. D.; et al. Pharmacologic inhibition of site 1 protease activity inhibits sterol regulatory element-binding protein processing and reduces lipogenic enzyme gene expression and lipid synthesis in cultured cells and experimental animals. *J. Pharmacol. Exp. Ther.* **2008**, *326*, 801−808.
(31) Chanas, S. A.; Jiang, Q.; McMahon, M.; McWalter, G. K.; McLellan, L. I.; Elcombe, C. R.; Henderson, C. J.; Wolf, C. R.; Moffat, G. J.; Itoh, K.; et al. Loss of the Nrf2 transcription factor causes a marked reduction in constitutive and inducible expression of the glutathione S-transferase Gsta1, Gsta2, Gstm1, Gstm2, Gstm3 and Gstm4 genes in the livers of male and female mice. *Biochem. J.* **2002**, *365*, 405−416.
(32) Chen, Q. M.; Maltagliati, A. J. Nrf2 at the heart of oxidative stress and cardiac protection. *Physiol. Genomics* **2018**, *50*, 77−97.
(33) Hayes, J. D.; Dinkova-Kostova, A. T. The Nrf2 regulatory network provides an interface between redox and intermediary metabolism. *Trends Biochem. Sci.* **2014**, *39*, 199−218.
(34) Grandjean, J. M. D.; Plate, L.; Morimoto, R. I.; Bollong, M. J.; Powers, E. T.; Wiseman, R. L. Deconvoluting Stress-Responsive Proteostasis Signaling Pathways for Pharmacologic Activation Using Targeted RNA Sequencing. *ACS Chem. Biol.* **2019**, *14*, 784−795.
(35) Ibrahim, L.; Mesgarzadeh, J.; Xu, I.; Powers, E. T.; Wiseman, R. L.; Bollong, M. J. Defining the Functional Targets of Cap'n'collar Transcription Factors NRF1, NRF2, and NRF3. *Antioxidants* **2020**, *9*, No. 1025.
(36) Itoh, K.; Chiba, T.; Takahashi, S.; Ishii, T.; Igarashi, K.; Katoh, Y.; Oyake, T.; Hayashi, N.; Satoh, K.; Hatayama, I.; et al. An Nrf2/Small Maf Heterodimer Mediates the Induction of Phase II Detoxifying Enzyme Genes through Antioxidant Response Elements. *Biochem. Biophys. Res. Commun.* **1997**, *236*, 313−322.
(37) Brandes, M. S.; Gray, N. E. NRF2 as a Therapeutic Target in Neurodegenerative Diseases. *ASN Neuro* **2020**, *12*, No. 1759091419899782.
(38) Lewerenz, J.; Albrecht, P.; Tien, M. L.; Henke, N.; Karumbayaram, S.; Kornblum, H. I.; Wiedau-Pazos, M.; Schubert, D.; Maher, P.; Methner, A. Induction of Nrf2 and xCT are involved in the action of the neuroprotective antibiotic ceftriaxone in vitro. *J. Neurochem.* **2009**, *111*, 332−343.
(39) Singh, A.; Venkannagari, S.; Oh, K. H.; Zhang, Y. Q.; Rohde, J. M.; Liu, L.; Nimmagadda, S.; Sudini, K.; Brimacombe, K. R.; Gajghate, S.; et al. Small Molecule Inhibitor of NRF2 Selectively Intervenes Therapeutic Resistance in KEAP1-Deficient NSCLC Tumors. *ACS Chem. Biol.* **2016**, *11*, 3214−3225.
(40) Canning, P.; Sorrell, F. J.; Bullock, A. N. Structural basis of Keap1 interactions with Nrf2. *Free Radical Biol. Med.* **2015**, *88*, 101−107.
(41) Zhang, D. D.; Hannink, M. Distinct cysteine residues in Keap1 are required for Keap1-dependent ubiquitination of Nrf2 and for stabilization of Nrf2 by chemopreventive agents and oxidative stress. *Mol. Cell. Biol.* **2003**, *23*, 8137−8151.
(42) Fischer, W.; Currais, A.; Liang, Z.; Pinto, A.; Maher, P. Old age-associated phenotypic screening for Alzheimer's disease drug candidates identifies sterubin as a potent neuroprotective compound from Yerba santa. *Redox Biol.* **2019**, *21*, No. 101089.
(43) Bollong, M. J.; Lee, G.; Coukos, J. S.; Yun, H.; Zambaldo, C.; Chang, J. W.; Chin, E. N.; Ahmad, I.; Chatterjee, A. K.; Lairson, L. L.; et al. A metabolite-derived protein modification integrates glycolysis with KEAP1-NRF2 signalling. *Nature* **2018**, *562*, 600−604.
(44) Riss, T. L. M. R.; Niles, A. L. et al. Cell Viability Assays. In *Assay Guidance Manual Bethesda (MD)*; Markossian, S. S. G.; Grossman, A. et al., Eds.; Eli Lilly & Company and the National Center for Advancing Translational Sciences, 2013.
(45) Grandjean, J. M. D.; Madhavan, A.; Cech, L.; Seguinot, B. O.; Paxman, R. J.; Smith, E.; Scampavia, L.; Powers, E. T.; Cooley, C. B.; Plate, L.; et al. Pharmacologic IRE1/XBP1s activation confers targeted ER proteostasis reprogramming. *Nat. Chem. Biol.* **2020**, *16*, 1052−1061.

https://doi.org/10.1021/acschembio.1c00810
ACS Chem. Biol. 2021, 16, 2852−2863